Raman Spectrum of Single-Domain $BaTiO_3$

M. DiDomenico, Jr., S. H. Wemple, and S. P. S. Porto*
Bell Telephone Laboratories, Murray Hill, New Jersey 07974
AND
R. P. Bauman
Department of Physics, University of Alabama, Birmingham, Alabama
(Received 5 April 1968)

Room-temperature Raman spectra of high-quality single-domain $BaTiO_3$ crystals are reported. The frequencies of the Raman-active long-wavelength optical phonons are determined and shown to be in reasonable agreement with the Lyddane-Sachs-Teller (LST) relation as well as infrared reflectivity data. The effects of mode damping on the Raman line shape are discussed using a classical lattice-polarization-fluctuation model for the Raman scattering process. Based on this model, it is shown that the soft E mode is overdamped, and at 25°C has an undamped mode frequency ω_{TO} of 36 ± 3 cm^{-1} and a damping constant Γ of 1.1 ± 0.1. The temperature dependence of ω_{TO} is given and found to be consistent with the LST relation. The soft A_1 mode is not observed, but is estimated from the LST relation and infrared reflectivity data to be heavily damped ($\Gamma\approx0.5$) and to have an undamped mode frequency of 180 ± 10 cm^{-1}.

I. INTRODUCTION

Because of the close relationship between ferroelectricity and lattice dynamics, Raman spectroscopy provides a potentially valuable technique for the study of ferroelectric materials. Of major interest is the dynamical behavior of the lowest-frequency transverse optical (TO) mode, whose frequency was predicted by Cochran[1] and Anderson[2] to be strongly temperature-dependent. The expected temperature dependence of this "soft mode" has been observed in $SrTiO_3$ and $KTaO_3$ from infrared reflectivity[3–5] and inelastic neutron scattering[6,7] experiments. Results for $BaTiO_3$ are not as clear cut, however, because of experimental difficulties, and also because the soft mode appears to be overdamped.[8–10] Recent neutron scattering data of Shirane *et al.*[11] yield frequencies of the lowest TO branch in $BaTiO_3$ which are considerably below those expected for an undamped mode as predicted by the Lyddane-Sachs-Teller (LST) relation.[12,13]

In this paper we report measurements of the Raman spectrum of a large single-domain $BaTiO_3$ crystal at 25°C using well-defined scattering geometries so that symmetry assignments of all the modes can be made. The temperature dependence and line shape of the soft E mode has also been measured in the ferroelectric phase and related to a scattering model which allows a determination of both the *undamped* mode frequency and the damping factor. An analysis of these data which shows that the soft mode is indeed *overdamped* in $BaTiO_3$ has been reported previously.[14]

Several earlier studies of the Raman effect in $BaTiO_3$ are either inconsistent or of limited usefulness because multiple-domain samples and undefined scattering geometries were used.[15–17] Pinczuk *et al.*[18] and Parsons and Rimai[19] report measurements on single-domain crystals, but not all the expected modes were observed, some incorrect assignments were made, and the observed modes were apparently not consistent with the LST relation. Furthermore, Pinczuk *et al.* did not relate the unusually broad soft E mode line shape to the effects of overdamping. Measurements of the temperature dependence of the Raman spectrum reported by Parsons and Rimai show strong peaks in both the tetragonal and cubic phases of $BaTiO_3$, even though symmetry precludes the observation of first-order spectra in the cubic phase. These results suggest that care must be taken to separate first-order spectra from a strong higher-order background. The unusual strength of higher-order spectra in perovskite ferroelectrics has been noted in $SrTiO_3$ [20] and $KTaO_3$.[21] However, electric

* Present address: Department of Physics and Electrical Engineering, University of Southern California, Los Angeles, Calif.

[1] W. Cochran, Advan. Phys. **9**, 387 (1960).
[2] P. W. Anderson, in *Proceedings of the All-Union Conference on the Physics of Dielectrics* (Academy of Sciences, USSR, Moscow, 1958), p. 290.
[3] A. S. Barker, Jr., and M. Tinkham, Phys. Rev. **125**, 1527 (1962).
[4] R. C. Miller and W. G. Spitzer, Phys. Rev. **129**, 94 (1963).
[5] C. H. Perry and T. F. McNally, Phys. Rev. **154**, 459 (1967).
[6] R. A. Cowley, Phys. Rev. **134**, A981 (1964).
[7] G. Shirane, R. Nathans, and V. J. Minkiewicz, Phys. Rev. **157**, 396 (1967).
[8] W. G. Spitzer, R. C. Miller, D. A. Kleinman, and L. E. Howarth, Phys. Rev. **126**, 1710 (1962).
[9] J. M. Ballantyne, Phys. Rev. **136**, A429 (1964).
[10] A. S. Barker, Jr., Phys. Rev. **145**, 391 (1966).
[11] G. Shirane, B. C. Frazer, V. J. Minkiewicz, J. A. Leake, and A. Linz, Phys. Rev. Letters **19**, 234 (1967).
[12] R. H. Lyddane, R. G. Sachs, and E. Teller, Phys. Rev. **59**, 673 (1941).
[13] A. S. Barker, Jr., Phys. Rev. **136**, A1290 (1964).
[14] M. DiDomenico, Jr., S. P. S. Porto, and S. H. Wemple, Phys. Rev. Letters **19**, 855 (1967).
[15] Y. S. Bobovich and E. V. Bursian, Opt. i Spetroskopiya **11**, 131 (1961) [English transl.: Opt. Spectry. (USSR) **11**, 69 (1961)].
[16] S. Ikegami, J. Phys. Soc. Japan **19**, 46 (1964).
[17] C. H. Perry and D. B. Hall, Phys. Rev. Letters **15**, 700 (1965).
[18] A. Pinczuk, W. Taylor, E. Burstein, and I. Lefkowitz, Solid State Commun. **5**, 429 (1967).
[19] J. L. Parsons and L. Rimai, Solid State Commun. **5**, 423 (1967).
[20] W. G. Nilsen and J. G. Skinner, J. Chem. Phys. **48**, 2240 (1968).
[21] W. G. Nilsen and J. G. Skinner, J. Chem. Phys. **47**, 1413 (1967).

field induced first-order Raman spectra have been observed in these materials in their cubic phases by Fleury and Worlock.[22] Dvorak[23] has investigated theoretically the first-order Raman scattering induced in cubic perovskite ferroelectrics by the application of a static electric field.

II. EXPERIMENTAL

The experimental arrangement has been described previously by Damen *et al.*[24] It consists of a sectioned metal-bore ion laser tube, a laser focusing lens, light collection optics, a Spex model 1400 double monochromater, a photomultiplier, and detecting electronics. The metal-bore ion laser could be used with either argon or krypton, and with a Brewster angle prism inserted in the laser cavity nearly two dozen laser lines could be selected. Using argon, we obtained approximately 200 mW of power in either the 4880- or 5145-Å lines. For most experiments the 4880-Å laser line was focused into the $BaTiO_3$ sample using a 10-cm focal length lens, and the scattered radiation was collected by $f/1$ optics which matched the $f/6.8$ optics of the spectrometer. The slit widths used for most spectra corresponded to resolutions of about 6 cm^{-1}; however, for the very strong lowest-frequency E mode the slits were reduced to give approximately 0.5-cm^{-1} resolution, thereby enabling us to measure the Raman spectrum close to the exciting line. In all cases the images of the points where the laser enters and exits the sample were masked off at the spectrometer entrance slit.

An EMI-6256 S photomultiplier (S-11 surface) cooled to about $-50°C$ was used as a detector. Pulses from the photomultiplier were counted with photon counting electronics, integrated and amplified by an electrometer, and recorded. The photomultiplier dark current corresponded to 1–2 photoelectrons per second so that most of the noise in our spectra was a result of photon noise associated with the Poisson distribution of the time of arrival of photons at the photomultiplier surface. Integration times were usually 1 sec.

III. CRYSTAL PREPARATION AND DIELECTRIC PROPERTIES

The $BaTiO_3$ crystal used in these experiments was grown by a top-seeded solution growth method[25] involving a stoichiometric excess of TiO_2. With this method no extraneous flux is used so that crystals are thought to be considerably purer than flux-grown platelets. Evidence for higher purity in our samples is provided by optical-absorption experiments which show considerably lower absorption than in flux-grown samples in the vicinity of the interband edge.[26] Also, the Curie temperature of our sample is $\approx 133°C$,[27,28] rather than the normally quoted value of 120°C. Since high optical quality single-domain crystals are required for the Raman scattering experiments, care was taken to properly pole the sample. This was accomplished by heating above the 133°C cubic-tetragonal transition in an oil bath, applying a dc field of several kV/cm along a ⟨100⟩ axis, and then cooling slowly through the transition in the presence of the field. Following this procedure, surface cracks generally formed; these were subsequently removed using a string saw. The final dimensions of our polished single-domain crystal were $5.2 \times 4.9 \times 2.6$ mm^3.

It is of interest to compare the optical mode vibrational frequencies determined from Raman spectra with the low- and high-frequency dielectric constants via the LST relation, especially in view of inconsistencies reported recently in the literature.[18,19] To do this, we have measured the low-frequency dielectric constant of our single-domain $BaTiO_3$ crystal both parallel (c axis) and perpendicular (a axis) to the spontaneous polarization direction. Results[28] at 25°C for a frequency below all piezoelectric resonances (100 kHz) and for a frequency above these resonances (250 MHz) are

$$\epsilon_a'(100\text{ kHz}) = 3600; \qquad \epsilon_a'(250\text{ MHz}) = 2300;$$

$$\epsilon_c'(100\text{ kHz}) = 150; \qquad \epsilon_c'(250\text{ MHz}) = 80.$$

The measurements at 100 kHz were made using a Boonton capacitance bridge, and those at 250 MHz were made with a Boonton RX meter. It is clear that a large piezoelectric clamping effect is present. The appropriate dielectric constant to be used in the LST relation is, of course, the clamped value since all frequency shifts observed in the Raman scattering experiment are very much greater than the piezoelectric resonance frequencies. Our dielectric-constant data[28] differ somewhat from previously reported results,[29,30] probably because our sample is of higher purity and therefore has a higher cubic-tetragonal transition temperature ($T_c = 1.33°C$), and a higher tetragonal-orthorhombic transition temperature ($T = 6°C$) than the flux-grown crystals previously investigated. Values of the high-frequency (optical) dielectric constant to be incorporated into the LST relation have been obtained from new refractive-index data[28] by extrapolating a single-term Sellmeier dispersion relation to infinite wavelength. Using this procedure we obtain $\epsilon_a(\infty) = 5.22$ and $\epsilon_c(\infty) = 5.07$. These data are higher than reported by Shumate[31] for flux-grown crystals.

[22] P. A. Fleury and J. M. Worlock, Phys. Rev. Letters **18**, 665 (1967).
[23] V. Dvorak, Phys. Rev. **159**, 652 (1967).
[24] T. C. Damen, S. P. S. Porto, and B. Tell, Phys. Rev. **142**, 570 (1966).
[25] A. Linz, V. Belruss, and C. S. Naiman, J. Electrochem. Soc. **112**, 60C (1965).
[26] M. DiDomenico, Jr., and S. H. Wemple, Phys. Rev. **166**, 565 (1968).
[27] C. J. Johnson, Appl. Phys. Letters **7**, 221 (1965).
[28] S. H. Wemple, M. DiDomenico, Jr., and I. Camlibel, J. Phys. Chem. Solids (to be published).
[29] T. S. Benedict and J. L. Durand, Phys. Rev. **109**, 1091 (1958).
[30] D. Berlincourt and H. Jaffe, Phys. Rev. **111**, 143 (1958).
[31] M. S. Shumate, Appl. Phys. Letters **5**, 178 (1964).

IV. LATTICE VIBRATIONAL MODES IN $BaTiO_3$

$BaTiO_3$ has five atoms and fifteen degrees of freedom per unit cell. Above the cubic-tetragonal transition at 133°C it has O_h symmetry, and the 15 degrees of freedom are therefore divisible into the representations $4F_{1u}+1F_{2u}$. One of the F_{1u} symmetry modes corresponds to the acoustical branch while the remaining representations $3F_{1u}+1F_{2u}$ belong to the optical branches. The F_{1u} modes in cubic $BaTiO_3$ are infrared active, whereas the F_{2u} mode is inactive, but both F_{1u} and F_{2u} symmetry modes are Raman inactive so that there is no first-order Raman effect in $BaTiO_3$ above its Curie temperature. Between 133 and 6°C, where $BaTiO_3$ is tetragonal and has C_{4v} symmetry, each of the F_{1u} modes splits into modes of symmetry A_1+E, and the F_{2u} mode splits into modes of symmetry B_1+E. The A_1 phonon modes are infrared active for the extraordinary ray (c- or z-axis polarization), while the E modes are infrared active for the ordinary ray [a- or $x(y)$-axis polarization]. The B_1 symmetry mode is infrared inactive in both the cubic and tetragonal phases of $BaTiO_3$. However, all the optical phonons of $BaTiO_3$ are first-order Raman active in the C_{4v} phase with the following polarizability tensors α associated with each of the modes[32]:

$$\alpha[A_1(z)]=\begin{pmatrix} a & 0 & 0 \\ 0 & a & 0 \\ 0 & 0 & b \end{pmatrix}, \qquad \alpha[B_1]=\begin{pmatrix} c & 0 & 0 \\ 0 & -c & 0 \\ 0 & 0 & 0 \end{pmatrix},$$

$$\alpha[E(x)]=\begin{pmatrix} 0 & 0 & d \\ 0 & 0 & 0 \\ d & 0 & 0 \end{pmatrix}, \qquad \alpha[E(y)]=\begin{pmatrix} 0 & 0 & 0 \\ 0 & 0 & d \\ 0 & d & 0 \end{pmatrix},$$

where x, y, and z refer to the axis of light polarization. Based on the above analysis we conclude that the displacive ferroelectric phase transition $O_h \rightarrow C_{4v}$ changes the irreducible representation from

$$3F_{1u}(\text{optical})+1F_{2u}(\text{optical})+1F_{1u}(\text{acoustic})$$

to

$$3A_1(\text{optical})+1B_1(\text{optical})+4E(\text{optical}) \\ +1A_1(\text{acoustic})+1E(\text{acoustic}).$$

There are further splittings of the vibrational modes due to long-range electrostatic forces associated with lattice ionicity; as a consequence, each of the infrared active modes of symmetry A_1 and E splits into pairs of modes, i.e., $A_1 \rightarrow A_1(\text{TO})+A_1(\text{LO})$ and $E \rightarrow E(\text{TO})+E(\text{LO})$, where TO and LO refer, respectively, to transverse optic and longitudinal optic. Because the E symmetry mode connected with F_{2u} was not observed by Spitzer *et al.*[8] in the infrared reflectivity of tetragonal $BaTiO_3$, we can reasonably assume that the oscillator strength, and therefore the LO-TO splitting, is small for this mode. We then obtain the following distinct Raman-active optical lattice vibrations for $BaTiO_3$ in its tetragonal phase: $3A_1(\text{TO})+3A_1(\text{LO})+3E(\text{TO})+3E(\text{LO})+1E(\text{LO}+\text{TO})+1B_1$. Further splittings can occur due to anisotropy of the short-range force constants as evidenced by the anisotropic dielectric behavior. Each of the phonons propagating in the z direction can consequently have a different frequency from those propagating in the xy plane. As a final result, we obtain the following 18 expected long-wavelength first-order Raman-active optical phonons in the C_{4v} phase of $BaTiO_3$:

$$3A_1(\text{TO}, xy)+3A_1(\text{LO}, z)+3E(\text{TO}, xy)+3E(\text{TO}, z) \\ +3E(\text{LO}, xy)+1E(\text{TO}+\text{LO}, xy) \\ +1E(\text{TO}+\text{LO}, z)+1B_1.$$

Our notation gives the mode symmetry followed in parentheses by the type of mode and direction of propagation, e.g., $A_1(\text{TO}, xy)$ denotes an A_1 symmetry TO mode propagating in the xy plane. There may, of course, be near degeneracies between a number of these permitted modes. For example, the $E(\text{TO}, xy)$ and $E(\text{TO}, z)$ modes are degenerate at the zone center, and A_1 and E modes with the same propagation direction may not be too different, as evidenced by the similarity between the ordinary and extraordinary ray infrared reflectivity spectra measured by Spitzer *et al.*[8] Furthermore, as we shall show, all the modes derived from the cubic F_{2u} mode, i.e., $1E(\text{TO}+\text{LO}, xy)+1E(\text{TO}+\text{LO}, z)+1B_1$, are essentially degenerate.

The presence of a strong second- and higher-order Raman effect in $BaTiO_3$ complicates the first-order Raman-active mode picture given above. The data of Perry and Hall[17] and Parsons and Rimai[19] show a Raman spectrum above the Curie temperature in the cubic phase which remains in the ferroelectric phase. The existence of a strong second-order spectrum in the cubic phases of $SrTiO_3$ and $KTaO_3$ has been reported by Nilsen and Skinner.[20,21] A similarity between higher-order Raman spectra in $BaTiO_3$ and $SrTiO_3$ is to be expected since, except for the soft TO mode, they exhibit similar lattice dynamical behavior.[6,11] For example, the zone-boundary frequency of the transverse acoustic (TA) phonon falls at approximately 115 cm^{-1} in both materials so that the strong 2 TA two-phonon process at 230 cm^{-1} observed in $SrTiO_3$ is also expected in $BaTiO_3$. More specifically, we expect in $BaTiO_3$ rather broad higher-order bands at 250–350 cm^{-1} and at 500–650 cm^{-1} based on the results for $SrTiO_3$. We believe that these are the two bands observed by Parsons and Rimai[19] both above and below the Curie temperature in $BaTiO_3$ and that they can be attributed to Raman scattering processes higher than first order.

[32] R. Loudon, Advan. Phys. **13**, 423 (1964).

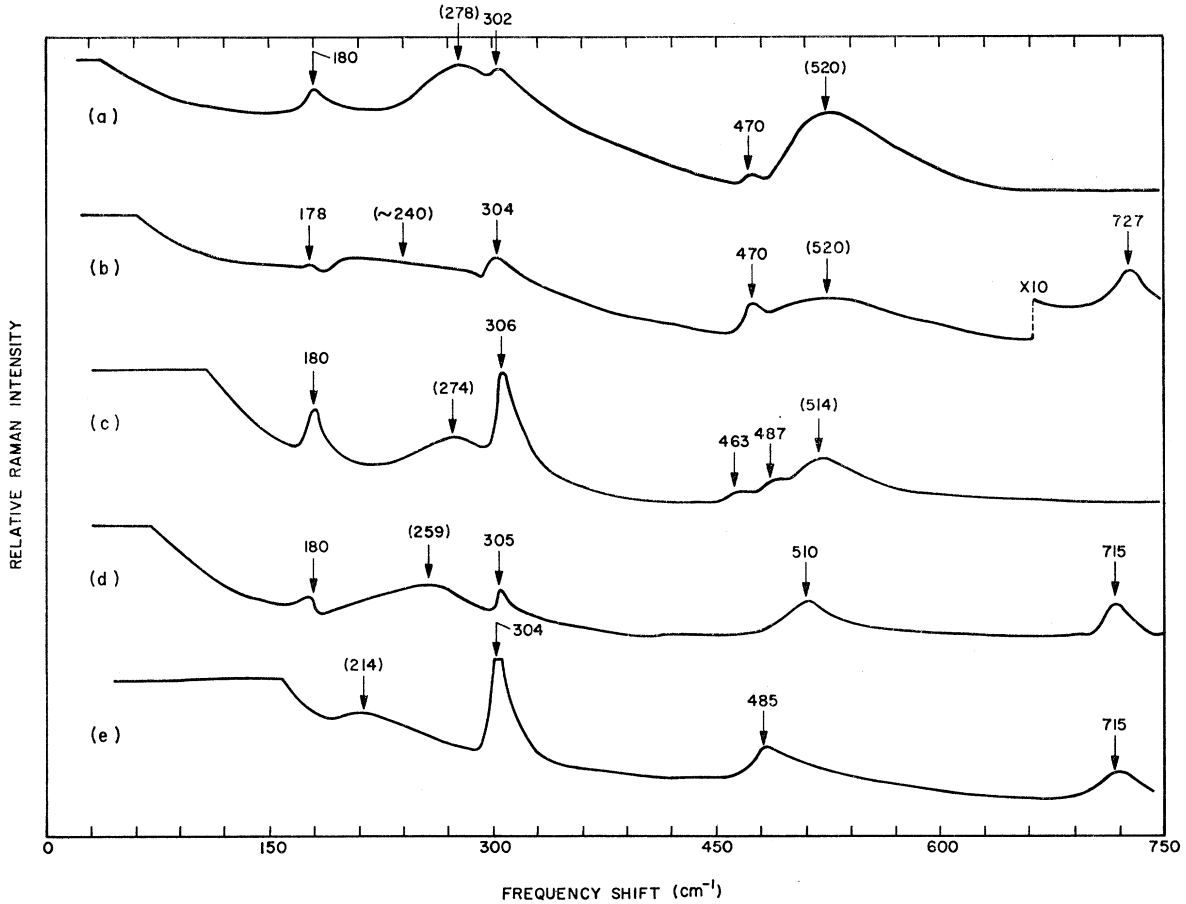

FIG. 1. Raman spectra (Stokes components) of single-domain $BaTiO_3$ at 25°C. (a) $(\mathbf{X}+\mathbf{Z})(yy)(-\mathbf{X}+\mathbf{Z})$ spectrum, (b) $(\mathbf{X}+\mathbf{Z})(yy)(\mathbf{X}-\mathbf{Z})$ spectrum, (c) $\mathbf{X}(yz)\mathbf{Y}$ spectrum, (d) $(\mathbf{X}+\mathbf{Z})(xz)(\mathbf{X}-\mathbf{Z})$ spectrum, and (e) $\mathbf{Y}(zx)\mathbf{Z}$ spectrum. Higher-order bands are identified in parentheses. The resolution is about 6 cm^{-1}.

V. RESULTS

To describe the first-order Raman scattering observed in $BaTiO_3$, we use a nomenclature similar to that introduced by Damen *et al.*[24] A spectrum labeled $\mathbf{X}(yy)\mathbf{Z}$, for example, means that both the incident radiation traveling in the direction **X** and the scattered radiation traveling in the direction **Z** are polarized in the y direction; this spectrum is therefore determined by the α_{yy} polarizability tensor component for a phonon propagating in the xz plane at 45° to the x or z axis. Figure 1 shows Stokes components of the Raman spectra of single-domain $BaTiO_3$ at 25°C for various scattering geometries. In Fig. 1(a) we show the $(\mathbf{X}+\mathbf{Z})(yy)(-\mathbf{X}+\mathbf{Z})$ spectrum which gives the $A_1(\mathrm{TO}, xy)$ phonon modes. In this notation $(\mathbf{X}+\mathbf{Z})$ means that radiation is traveling in the xz plane at 45° to the x or z axis. Two modes are evident at 180 and 470 cm^{-1} as well as the B_1 mode at 302 cm^{-1}. The low-frequency $A_1(\mathrm{TO}, xy)$ mode is absent, probably as a result of the strong and very broad higher-order band which peaks at approximately 278 cm^{-1}. We show below using the LST relation that the undamped frequency of this mode should occur near 180 cm^{-1}. Figure 1(a) also shows another strong higher-order band at about 520 cm^{-1}. Both the 278 and 520 cm^{-1} bands were observed by Parsons and Rimai[19] in the cubic phase. The $(\mathbf{X}+\mathbf{Z})(yy)(\mathbf{X}-\mathbf{Z})$ spectrum of Fig. 1(b) shows the $A_1(\mathrm{LO}, z)$ modes at 178, 470, and 727 cm^{-1} as well as the B_1 mode at 304 cm^{-1}. Figure 1(c) gives the $\mathbf{X}(yz)\mathbf{Y}$ spectrum which corresponds to $E(\mathrm{TO}, xy)$ and $E(\mathrm{LO}, xy)$ modes. In this spectrum the 180-cm^{-1} band is $E(\mathrm{TO})+E(\mathrm{LO})$; the 463-$cm^{-1}$ band is $E(\mathrm{LO}, xy)$; the 487-cm^{-1} band is $E(\mathrm{TO}, xy)$; the 306-cm^{-1} band is an E mode derived from the F_{2u} cubic mode; and the broad bands at approximately 274 and 514 cm^{-1} are due to higher-order processes. In the spectrum of Fig. 1(c) we should also see an additional $E(\mathrm{LO}, xy)$ mode in the vicinity of 720 cm^{-1}. This mode is missing, but appears to be present at 715 cm^{-1} in the $(\mathbf{X}+\mathbf{Z})(xy)(\mathbf{X}-\mathbf{Z})$ spectrum of Fig. 1(d) which should give principally $E(\mathrm{TO}, z)$ phonon modes. In addition to the 305-cm^{-1} E mode coming from the F_{2u} cubic mode, this spectrum gives E modes at (1) 180 cm^{-1}—

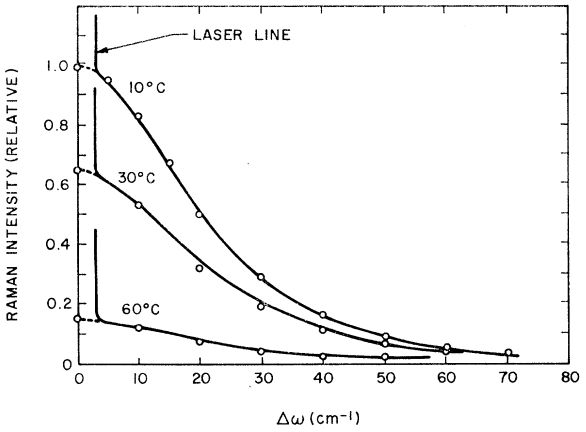

FIG. 2. Stokes components of the soft E mode Raman spectra in single-domain $BaTiO_3$ at temperatures of 10, 30, and 60°C. The spectra were obtained with the $\mathbf{X}(zy)(-\mathbf{X})$ scattering geometry using spectral slit widths of $\approx\frac{1}{2}$ cm^{-1}. The spectra were normalized with respect to the zero-frequency amplitude of the 10°C spectrum. The open circle points give the best oscillator fit using the parameters listed in Table II.

the shape and position of this mode are obscured somewhat by interference with the higher-order band at 259 cm^{-1}; (2) 510 cm^{-1}—this mode appears in the vicinity of the higher-order band at approximately 515–520 cm^{-1} making a definite assignment difficult; however, we speculate on the basis of line shape that a one-phonon $E(\mathrm{TO}, z)$ band falls in the vicinity of 510 cm^{-1}. In Fig. 1(e) we give the $\mathbf{Y}(zx)\mathbf{Z}$ spectrum showing the $E(\mathrm{TO}, xy)$ mode at 485 cm^{-1}, the $E(\mathrm{LO}, xy)$ mode at 715 cm^{-1}, and the cubic F_{2u} $E(\mathrm{TO}+\mathrm{LO})$ mode at 304 cm^{-1}. All of the spectra shown in Fig. 1 were recorded with spectral slit widths of 6 cm^{-1} in order to observe the weak bands. As a result, long tails were observed near the laser exciting line.

The presence of $E(\mathrm{TO})$ phonons very close to the laser line can be observed by reducing the spectral slit width to approximately $\frac{1}{2}$ cm^{-1}. When this is done the low-resolution wings occuring near the laser line in Fig. 1 disappear, and we find that spectra can be recorded to within approximately 3 cm^{-1} of the exciting line. In high resolution the A_1 modes show no structure near the exciting line. However, for the low-frequency $E(\mathrm{TO}, xy)$ phonon modes a broad nonresonant line shape is observed extending out from the laser line. In Fig. 2 we show composites of the $\mathbf{X}(zy)(-\mathbf{X})$ Stokes spectra at temperatures of 10, 30, and 60°C. The base line and edge of the laser line were obtained from the $\mathbf{X}(zz)(-\mathbf{X})$ spectra which showed no structure. We point out that the Raman scattering efficiency of this soft $E(\mathrm{TO}, xy)$ mode was approximately 10^3 higher than obtained from the other phonons in $BaTiO_3$ so that the spectra could be readily recorded in high resolution. As reported previously[14] the nonresonant line shape shown in Fig. 2 is a consequence of having an overdamped phonon mode. We have extracted undamped mode frequencies from the data of Fig. 2 by fitting the Raman line shape

TABLE I. Optical-branch vibrational mode assignments in tetragonal $BaTiO_3$ at 25°C.

Cubic representation	Raman scattering data (cm^{-1}): accuracy ±3 cm^{-1}						Infrared data[a] (cm^{-1})		
	$E(\mathrm{TO}, xy)$	$E(\mathrm{TO}, z)$	$E(\mathrm{LO}, xy)$	$A_1(\mathrm{TO}, xy)$	$A_1(\mathrm{LO}, z)$	$E(\mathrm{TO}+\mathrm{LO}, xy)$	$E(\mathrm{TO}+\mathrm{LO}, z)$	B_1	$E(\mathrm{TO})$	$E(\mathrm{LO})$
F_{1u}	36[b]	36[b]	715	≈180[c]	727	...	...	...	34	704
F_{1u}	180	180	180	180	178	...	...	...	183	188
F_{1u}	486	518	463	470	470	...	...	...	500	463
F_{2u}	...	...	...	...	...	305	305	305	...	...

[a] Data taken from Ref. 8.
[b] These undamped mode frequencies were extracted from the observed nonresonant line shape (Fig. 2) as discussed in the text and in Ref. 14.
[c] This undamped frequency was determined from the LST relation and is estimated to be accurate to within ±10 cm^{-1}.

to a damped classical oscillator as described previously[14] and in more detail below.

VI. DISCUSSION

In Table I we list our assignments for the vibrational modes of tetragonal $BaTiO_3$ together with those determined from infrared reflectivity data. At 25°C, 16 distinct long-wavelength optical-branch frequencies have been identified. From our data we conclude that the splittings are small for most of the vibrational modes. The five modes, arising from the cubic F_{2u} symmetry mode, are all observed at approximately 305 cm^{-1} and must be considered degenerate. This is not surprising, because of the absence of this band in the infrared reflectivity spectra, as discussed above. The five predicted frequencies corresponding to an F_{1u} symmetry mode at 180 cm^{-1} also show negligibly small anisotropy and TO-LO splittings. Another F_{1u} mode, near 500 cm^{-1}, shows larger splittings. The higher-order contribution in this region is strongly evident and causes some of the positions to be uncertain. The LO modes of A_1 and E symmetry are nearly degenerate at $\approx$470 cm^{-1}, while the TO modes occur at slightly higher frequency, $\approx$500 cm^{-1}, as expected. The final cubic F_{1u} symmetry mode has very large TO-LO splittings, as well as large anisotropy splittings in the TO branch. The E(LO) mode is at 715 cm^{-1}, whereas the A_1(LO) mode is at 727 cm^{-1}. The soft E(TO) and A_1(TO) modes are shown below to be at $\approx$36 and $\approx$180 cm^{-1}, respectively. It should be noted that the mode positions given in Table I interlace properly as the mode frequency increases so that LO modes always occur at higher frequencies than TO modes.

Of major interest from the point of view of ferroelectricity is the soft E(TO) mode. The E(TO, xy) spectrum shown in Fig. 2 has a broad nonresonant line shape that can be simply related, by means of a classical oscillator model, to the undamped mode frequency and a damping factor. As discussed in the Appendix, the intensity of the Raman scattered light per unit frequency interval $dI_s/d\omega$ can be calculated in the classical limit from a thermodynamic polarization fluctuation model, which gives

$$dI_s/d\omega \propto kTP_s^2 I_l \epsilon''(\Delta\omega)/\Delta\omega, \tag{1}$$

where $\epsilon''(\Delta\omega)$ is the imaginary part of the dielectric dispersion function, $\Delta\omega$ is the frequency deviation from the laser exciting line, I_l is the laser intensity, P_s is the spontaneous polarization of the crystal, T is the temperature, and k is Boltzmann's constant. For a crystal having one dominant TO mode with undamped mode frequency ω_{TO} and damping factor Γ, the complex dielectric dispersion function may be written as

$$\epsilon(\omega)-\epsilon(\infty)=\frac{\epsilon'(0)\omega_{TO}^2}{(\omega_{TO}^2-\omega^2)+2i\Gamma\omega_{TO}\omega}, \tag{2}$$

where $\epsilon'(0)$ is the low-frequency clamped dielectric constant and $\epsilon(\infty)$ is the optical dielectric constant. Substituting Eq. (2) into Eq. (1) in the limit where $\epsilon(\omega)>\epsilon(\infty)$ yields

$$\frac{dI_s}{d\omega}\propto\frac{2kTP_s^2 I_l\Gamma\epsilon'(0)\omega_{TO}^3}{(\omega_{TO}^2-\Delta\omega^2)^2+4\Gamma^2\omega_{TO}^2\Delta\omega^2}. \tag{3}$$

The Raman spectra shown in Fig. 2 have been fitted to Eq. (3) by adjusting ω_{TO} and Γ; this procedure results in the undamped mode frequencies and damping factors listed in Table II. The open circles in Fig. 2 are the result of the curve-fitting procedure. The values of ω_{TO} and Γ are in excellent agreement with results of infrared reflectivity measurements.[8–10] For example, Barker[10] gives $\omega_{TO}=34$ cm^{-1} and $\Gamma=1.25$ at room temperature, whereas we find $\omega_{TO}\approx36$ cm^{-1} and $\Gamma\approx1.1$. The effect of damping on the Raman line shape as predicted by Eq. (3) is shown in Fig. 3. Curves are given for a lightly damped ($\Gamma\approx0$), a moderately damped ($0<\Gamma<1$), and a heavily damped ($\Gamma>1$) classical oscillator ($\Gamma=1$ for critical damping). The important point to be noted from these curves, apart from the changes in line shape, is that the frequency of the Raman peak is always shifted to a lower value by the presence of damping, and in particular for $\Gamma\geq0.707$ the peak is shifted to zero frequency. It is clear therefore that care must be taken in extracting mode frequencies from Raman spectra.

We now consider the temperature dependence of the Raman intensity of the soft E(TO) mode. From Eq. (3) we find using the LST relation $\epsilon'(0)\propto1/\omega_{TO}^2$ that the intensity at the peak of the line is given by

$$(dI_s/d\omega)_{\text{peak}}\propto kTP_s^2 I_l/4\Gamma(1-\Gamma^2)\omega_{TO}^3 \quad \text{for} \quad \Gamma<0.707 \tag{4a}$$

and

$$(dI_s/d\omega)_{\text{peak}}\propto kTP_s^2 I_l\Gamma/\omega_{TO}^3 \quad \text{for} \quad \Gamma>0.707. \tag{4b}$$

The frequency of the peak $\Delta\omega_p$ is

$$\Delta\omega_p=\omega_{TO}(1-2\Gamma^2)^{1/2} \quad \text{for} \quad \Gamma<0.707 \tag{5a}$$

and

$$\Delta\omega_p=0 \quad \text{for} \quad \Gamma>0.707. \tag{5b}$$

The total integrated Raman intensity I_s can be obtained from Eq. (1) by making use of the following Kramers-Kronig integral:

$$\epsilon'(\omega)=(2/\pi)\int_0^\infty\frac{\Delta\omega\epsilon''(\Delta\omega)}{\Delta\omega^2-\omega^2}d(\Delta\omega). \tag{6}$$

The result is

$$I_s\propto kTP_s^2 I_l/\omega_{TO}^2, \tag{7}$$

where we have made use of the LST relation $\epsilon'(0)\propto1/\omega_{TO}^2$. Equation (7) is the classical limit of the well-known quantum-mechanical result[32] $I_s\propto(N+1)/\omega_{TO}$ where N is the Bose population factor for the phonons. As shown in the Appendix the Raman line shape $dI_s/d\omega$ is proportional to the spectral density of the polarization

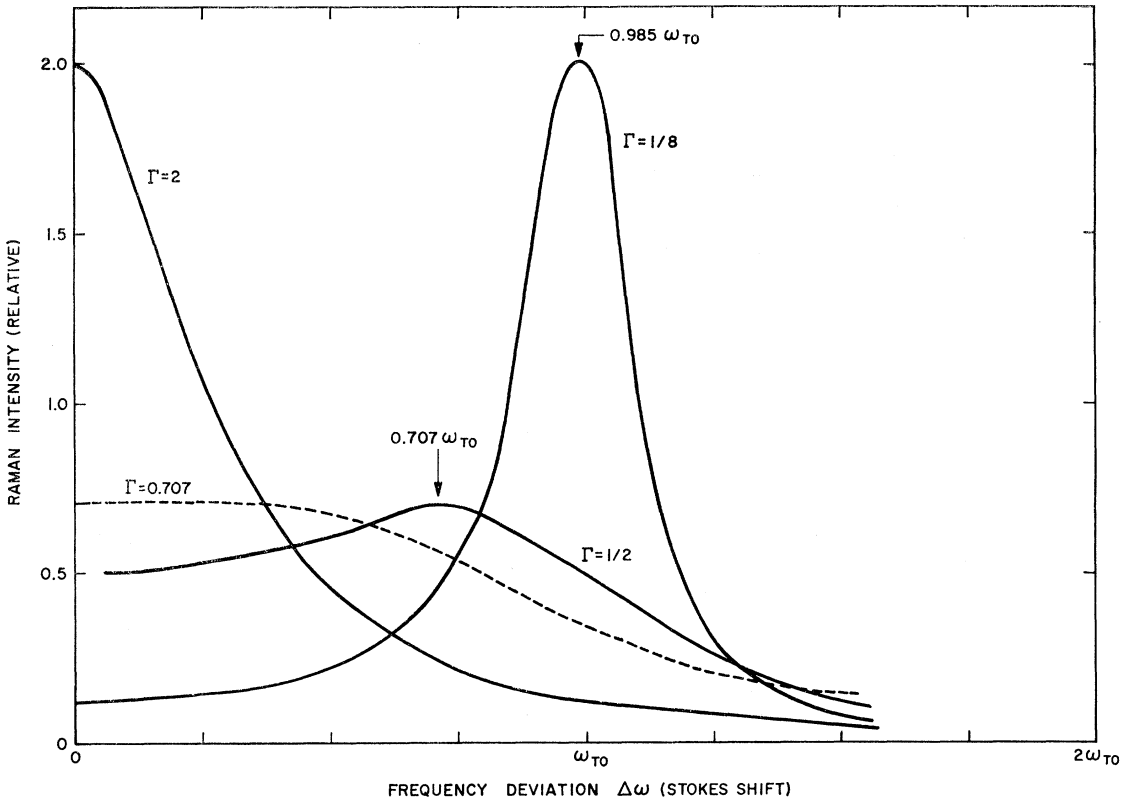

FIG. 3. Raman line shape in the presence of damping. Curves are plotted for a lightly damped $\Gamma=\frac{1}{8}$, a moderately damped $\Gamma=\frac{1}{2}$, and a heavily damped $\Gamma=2$ oscillator. Also shown is the line shape when $\Gamma=0.707$, a value which separates situations where the Raman peak is shifted to zero frequency ($\Gamma>0.707$) from those where the peak occurs at finite frequency ($\Gamma<0.707$). The curves are obtained from Eq. (3).

fluctuations given by

$$\langle P^2(\omega)\rangle=(4kT/V)[\epsilon''(\omega)/\omega], \tag{8}$$

where V is the volume. On the other hand, the integrated Raman intensity I_s measures the time-average polarization fluctuation $\langle p^2(t)\rangle$. This can be shown by using Parseval's theorem, i.e.,

$$\langle p^2(t)\rangle=(1/2\pi)\int_0^\infty \langle P^2(\omega)\rangle d\omega, \tag{9}$$

together with Eqs. (6) and (8), from which we obtain

$$\langle p^2(t)\rangle=kT\epsilon'(0)/V. \tag{10}$$

This result is well known in the thermodynamic theory of dielectric fluctuations.[33] By comparing Eqs. (7) and (10) and using the LST relation we obtain the result $I_s\propto\langle p^2(t)\rangle$. From this analysis we conclude that the integrated Raman intensity given by Eq. (7) is *independent of damping* and has a temperature dependence which follows TP_s^2/ω_{TO}^2. This behavior differs markedly from the behavior of the Raman intensity at the peak of the line which is directly affected by damping and which has a more complex temperature dependence given by Eqs. (4).

Using the soft mode oscillator parameters ω_{TO} and Γ listed in Table II, we compare the temperature dependence of the measured Raman intensity at $\Delta\omega=0$ with the dependence predicted by Eq. (4b). Taking previously measured[28] values of P_s (i.e., $P_s=0.26$ C/m^2 at 10°C, $P_s=0.25$ C/m^2 at 30°C, and $P_s=0.235$ C/m^2 at 60°C) we obtain the calculated results in Table II. The measured Raman intensity at 60°C may be somewhat low because of the presence of domain walls nucleating at this and higher temperatures. We find at 90°C, for example, that the crystal becomes almost entirely multiple domain, and that the Raman signal drops to nearly zero. The measured and calculated Raman intensities given in Table II are in agreement to within the error bars despite the uncertain influence of domains at 60°C. No domains were present at 10 and 30°C. We conclude therefore that the polarization fluctuation theory described in the Appendix accounts for the soft E mode Raman line shape as well as its temperature dependence, and that the broad nonresonant line shape peaking at $\Delta\omega=0$ is a consequence of overdamping of this mode.

[33] See, for example, *Fluctuation Phenomena in Solids*, edited by R. E. Burgess (Academic Press Inc., New York, 1965).

We now turn to the relationship between the observed Raman spectrum of $BaTiO_3$ and the dielectric behavior via the LST relation. It is important to recognize that the *undamped* mode frequencies are the appropriate values to use in the LST relation.[10] From the generalized LST relation we have

$$\epsilon'(0)/\epsilon(\infty) = (\omega_{LO}^{(1)}/\omega_{TO}^{(1)})^2(\omega_{LO}^{(2)}/\omega_{TO}^{(2)})^2 \times(\omega_{LO}^{(3)}/\omega_{TO}^{(3)})^2, \quad (11)$$

where the superscripts (1), (2), and (3) denote the three optical-branch modes derived from the F_{1u} cubic phase modes. For the E modes propagating in the xy plane, taking $\epsilon_a(\infty)=5.22$ and the mode frequencies from Table I, we obtain from Eq. (11), $\epsilon_a'(0)=1950\pm 500$. The measured value is $\epsilon_a'(0)=2300$ so that the observed E mode frequencies are in reasonable quantitative agreement with the LST relation. Assuming that only the soft E mode frequency is temperature-dependent, we can make use of Table I and Eq. (11) to calculate the temperature dependence of $\epsilon_a'(0)$. We obtain $\epsilon_a'(0)=2200\pm 550$ at 10°C, $\epsilon_a'(0)=1700\pm 400$ at 30°C, $\epsilon_a'(0)=1050\pm 350$ at 60°C. These values compare with measured values of $\epsilon_a'(0)=2680$, 2210, and 1760 at 10, 30, and 60°C, respectively, The lack of agreement at higher temperatures suggests that the temperature dependence of modes other than the soft E mode should be considered.

Recent inelastic neutron scattering experiments reported by Shirane *et al.*[11] at 230 and 430°C give anomalously low frequencies for the soft E(TO) mode. These results are difficult to understand both in terms of our Raman results and the LST relation. At 430°C, for example, we expect $\omega_{TO}\approx 70$ cm^{-1} from the LST relation rather than 11 cm^{-1} as reported by Shirane *et al.* These authors speculate that the resonant line shape which they observe indicates that the mode is underdamped at 230 and 430°C and that the observed peak is the acutal mode frequency. Failure to satisfy the LST relation makes this conclusion difficult to accept. The possibility that damping causes the peak frequency to shift from 70 cm^{-1} down to 11 cm^{-1} is also difficult to understand in view of the relatively narrow linewidth observed in the neutron scattering experiments.

Since the soft A_1(TO) mode was not observed in our Raman spectra, we estimate its position at 25°C using the LST relation and the measured c-axis dielectric constants. Taking $\epsilon_c'(0)=80$, $\epsilon_c(\infty)=5.07$, and the A_1 mode frequencies listed in Table I, we calculate from Eq. (11) an undamped A_1(TO, xy) mode frequency of 180 ± 10 cm^{-1}. Because the vibrational motions of the soft A_1(TO) mode are similar to those of the soft E(TO) mode, we expect that the A_1(TO) mode may also be heavily damped. This would make observation of the mode difficult since its intensity would then be distributed over a large frequency interval. For example, according to Fig. 3 the spectrum would be spread between $\Delta\omega=0$ and $\Delta\omega\approx\omega_{TO}$ for $\Gamma\approx\frac{1}{2}$. The presence of the broad higher-order band in the vicinity of 250 cm^{-1} (see Fig. 1) makes it particularly difficult to observe a heavily damped mode in this region. Recently, Barker[34] observed a very strong and broad A_1 mode spread between 100 and 200 cm^{-1} using infrared reflectivity techniques. From a classical oscillator fit to the data he concludes that $\omega_{TO}=150\pm 50$ cm^{-1} and $\Gamma=0.5\pm 0.25$. Failure to observe the soft A_1(TO) mode in the Raman spectrum is thus readily understandable.

TABLE II. Oscillator parameters and relative Raman intensities of the soft E(TO, xy) mode in $BaTiO_3$.

Temperature (°C)	ω_{TO} (cm^{-1})	Γ	Relative Raman intensity at $\Delta\omega=0$ Measured	Calculated
10	34±3	1±0.1	1.0[a]	1.0[a]
30	39±4	1.2±0.2	0.65±0.05	0.8±0.3
60	50±8	1.4±0.3	0.15±0.05	0.4±0.3

[a] The relative intensities at 10°C were defined to have unit amplitude. As a result, the errors in the measured and calculated intensities at 30 and 60°C include the errors in the 10°C intensity.

VII. CONCLUSION

Using Raman scattering experiments we have determined the frequencies of the allowed Raman active long-wavelength optical modes in the tetragonal phase of $BaTiO_3$ at room temperature. The soft E mode is found to be overdamped at 25°C with a damping factor $\Gamma\approx 1.1$ and undamped mode frequency $\omega_{TO}\approx 36$ cm^{-1}. The soft A_1 mode which is not observed because of the interfering effects of a higher-order band is thought to be heavily damped ($\Gamma\approx 0.5$) and to have an undamped frequency $\omega_{TO}\approx 180$ cm^{-1}. The observed mode frequencies are in reasonable agreement with the Lyddane-Sachs-Teller relation and with infrared reflectivity results.

Note added in proof. A recent paper on the Raman spectrum of $BaTiO_3$ by L. Rimai, J. L. Parsons, J. T. Hickmott, and T. Nakamura, Phys. Rev. **168,** 623 (1968), gives experimental results which, apart from the soft E mode, are similar to those described in the present paper. Our interpretation differs, however, from that given by these authors in several important respects. The low-frequency peak which they observe near 10 cm^{-1} in the soft E mode spectrum is not consistent with our results. Thus Rimai *et al.* conclude, contrary to the present paper, that the soft E mode is underdamped with an undamped mode frequency at 12 cm^{-1}. This conclusion is in disagreement with both the Lyddane–Sachs–Teller relation and infrared reflectivity data. Finally, several of the Raman bands which we believe to be second order are assigned by Rimai *et al.* as first order. This also bears on the disagreement they observe with the Lyddane–Sachs–Teller relation.

[34] A. S. Barker, Jr. (unpublished results).

ACKNOWLEDGMENTS

We wish to thank A. S. Barker, Jr. for kindly providing us with his unpublished infrared-reflectivity data for the soft A_1(TO) mode, and for his suggestions on the analysis given in the Appendix. We also wish to thank L. E. Cheeseman and I. Camlibel for their experimental assistance. It is a pleasure to thank A. Linz of MIT for providing the high-quality $BaTiO_3$ crystals.

APPENDIX: RAMAN SCATTERING FROM LATTICE POLARIZATION FLUCTUATIONS IN FERROELECTRICS

In the classical limit where $\hbar\omega_{TO} \ll kT$ first-order Raman scattering from the TO vibrational modes in ferroelectric crystals can be described in terms of lattice polarization fluctuations. The instantaneous optical polarization $m(t)$ generated in the crystal by a laser exciting field may be represented by

$$m(t) \propto (\partial\alpha/\partial q)_0 q(t) E_l \cos\omega_l t, \tag{A1}$$

where $(\partial\alpha/\partial q)_0$ is the change in electronic polarizability with respect to the normal coordinate q around the equilibrium position, and E_l and ω_l are, respectively, the laser field strength and frequency. It is reasonable to assume that the instantaneous amplitude of the TO mode normal coordinate $q(t)$ is proportional to the lattice polarization fluctuation $p(t)$ where $p(t) = e^* q(t)/v$. e^* is an effective charge and v is the unit cell volume. By taking the Fourier transform of Eq. (A1) and calculating the average Raman scattered intensity per unit frequency $dI_s/d\omega$, we obtain

$$dI_s/d\omega \propto (\partial\alpha/\partial q)_0^2 I_l \langle P^2(\Delta\omega)\rangle, \tag{A2}$$

where I_l is the laser intensity, $\Delta\omega$ is the frequency deviation from the laser exciting line (Stokes shift), and $\langle P^2(\Delta\omega)\rangle$ is the spectral density of the lattice polarization fluctuations. Using the Nyquist theorem for a crystal in thermodynamic equilibrium at temperature T, the spectral density of the polarization-current fluctuations is given by[35]

$$\langle I^2(\omega)\rangle = 4kT \mathrm{Re} G(\omega), \tag{A3}$$

where $G(\omega)$ is the complex dielectric conductivity at frequency ω, and Re denotes the real part. By noting that $\langle I^2(\omega)\rangle = \omega^2 A^2 \langle P^2(\omega)\rangle$, and that $G(\omega) = i\omega\epsilon(\omega) A/l$, where $\epsilon(\omega)$ is the complex dielectric constant, and A and l are, respectively, the cross-sectional area and length of the crystal, we find upon substitution into Eq. (A3)

$$\langle P^2(\omega)\rangle = 4(kT/V)[\epsilon''(\omega)/\omega]. \tag{A4}$$

Here $\epsilon''(\omega)$ is the imaginary part of the complex dielectric dispersion function $\epsilon(\omega) = \epsilon'(\omega) - i\epsilon''(\omega)$ and $V = Al$ is the volume. Combining Eq. (A4) and the relation $(\partial\alpha/\partial q)_0 \propto P_s$ derived from symmetry with Eq. (A2) we obtain the result

$$dI_s/d\omega \propto kTP_s^2 I_l \epsilon''(\Delta\omega)/\Delta\omega, \tag{A5}$$

where P_s is the spontaneous polarization.

[35] This analysis was suggested by A. S. Barker, Jr.